PHYSICAL REVIEW B **76**, 184401 (2007)

Evidence for two disparate spin dynamic regimes within Fe-substituted $La_{0.7}Pb_{0.3}(Mn_{1-x}Fe_x)O_3$ ($0 \leqslant x \leqslant 0.2$) colossal magnetoresistive manganites: Neutron spin-echo measurements

Jon Gutiérrez and J. M. Barandiarán
Department of Electricity and Electronics, Faculty of Science and Technology, University of the Basque Country, UPV/EHU, P.O. Box 644, 48080 Bilbao, Spain

F. J. Bermejo*
Instituto de Estructura de la Materia, CSIC -Unidad de Investigación Asociada al Instituto de Estructura de la Materia, Madrid E-28006, Spain
and Department of Electricity and Electronics, Faculty of Science and Technology, University of the Basque Country, UPV/EHU, P.O. Box 644, 48080 Bilbao, Spain

Claudia Mondelli
CNR-INFM and CRS Soft, Institut Laue-Langevin, 6 rue Jules Horowitz, Boîte Postale 156x, 38042 Genoble Cedex 9, France

Pierpaolo Romano
Fundación Tekniker, Avenlda Otaola 20, P.K. 44, 20600 Eibar, Gipuzkoa, Spain

Peter Fouquet
Institut Laue Langevin, 6 rue Jules Horowitz, Boîte Postale 156x, Grenoble 38042 Cedex 9, France

Michael Monkenbusch
Institut für Fetskörperforschung, Forschungzentrum Jülich GmbH, 52425 Jülich, Germany
(Received 15 June 2007; revised manuscript received 3 September 2007; published 1 November 2007)

The spin dynamics of substituted colossal magnetoresistive (CMR) manganites of general formula $La_{0.7}Pb_{0.3}(Mn_{1-x}Fe_x)O_3$, $0 \leqslant x \leqslant 0.2$ is investigated by means of neutron spin-echo measurements. Substitution of Mn by Fe leads to a strong decrease of the temperature of macroscopic magnetic long-range ordering with a concomitant enhancement of the CMR effect. For $x=0.2$, a long-range-ordered state is not achieved as a result of the increase in antiferromagnetic interactions brought forward by Fe^{+3}-Mn couplings. The results display two relaxations having well separated decay constants. A fast process with a relaxation time of about 10 ps within the paramagnetic phase is found for all compositions. It shows a remarkably strong dependence with temperature and sample composition as the apparent activation energy for spin diffusion as well as the preexponential term exemplify. The physical origin of such a fast relaxation is assigned to heavily damped or overdamped spin waves (spin diffusion) on the basis of some signatures of excitations having finite frequencies found for the parent compound $La_{0.7}Pb_{0.3}MnO_3$ at temperatures just below T_c, together with preliminary data on the effect of Fe doping on the stiffness constant. A slower relaxation is present for all compositions. Its temperature dependence follows the behavior of the macroscopic magnetization, and its intensity grows within the ordered ferromagnetic state. Its physical origin is ascribed to collective reorientation of nanoscale ferromagnetic domains on the basis of the wave-vector dependence of its relaxation rate and amplitude.

DOI: 10.1103/PhysRevB.76.184401 PACS number(s): 75.25.+z, 75.30.Ds, 75.40.Gb, 75.47.Gk

I. INTRODUCTION

The current view on the structure of colossal magnetoresistive (CMR) manganites portrays them as characterized by relatively simple crystal structures,[1] which, because of the interplay of spin, electronic, and structural degrees of freedom, give rise to highly heterogeneous magnetic ordering patterns. These usually contain short-range-ordered regions which coexist with long-range-ordered domains even below the macroscopic magnetic ordering temperature T_c.[2] There have been some discussions in the past pertaining to the specifics of such ordering patterns,[3] although a general consensus seems to have been reached nowadays.[4,5] Nanoscale inhomogeneities are now thought to constitute an intrinsic feature of CMR materials and these can take a wide variety of forms comprising stripe, checkerboard, or far less ordered patterns.[4]

As regards dynamical features, the view to which many researchers have adhered to in recent years considers Jahn-Teller (JT) polaronic regions[6] as responsible for the coexistence of both diffusive and propagating (spin waves) spin motions, as most experiments have revealed to date.[7] Such a picture has recently been questioned by detailed studies on the dependence on hole doping of the JT distortion.[8] These show that contrary to previous studies, such a distortion decreases with increasing hole doping. As an alternative, models considering a strong interaction between the lattice and the ferromagnetically ordered carriers have been postulated[9] as a means to explain the significant magnon linewidths (i.e., damping terms) observed near the zone boundaries in experi-

ments carried out at low temperatures where JT effects are deemed to be small.

The spectrum of spin-wave excitations of many of these materials has been studied in quite some detail.[7,10–15] Ferromagnetic (FM) regions which coexist with short-ranged antiferromagnetic (AFM) regions have been evidenced.[16,17] The effects of AFM interactions on the propagation of spin waves are now beginning to be understood.[18,19] However, recent systematic studies of spin-wave excitations on ferromagnetic metallic manganites[20] carried out versus carrier concentration emphasize the inadequacy of current theoretical approaches to account for the spin dynamics within the entire doping regime.

In contrast to the wealth of details concerning spin waves, the spin-diffusion processes that lead to the appearance of a quasielastic component in the neutron-scattering spectrum have received less attention. The broad, central component appearing in single crystal studies,[21,22] typically spanning over several meV, was assigned to fluctuating Jahn-Teller polarons, for which the quasielastic width provided a measure of their lifetimes of several tens of femtoseconds. Pioneering high-resolution spectroscopy measurements by Heffner *et al.*[23] by means of the concurrent use of muon spectroscopy and neutron spin-echo measurements have revealed the presence of complex relaxation patterns in $La_{0.7}Ca_{0.3}MnO_3$, which were attributed to a diffusive component as well as to a localized mode of unknown origin. To explain the origin of quasielastic scattering, explicit calculations on the basis of a frustrated Kondo lattice model[24] have been carried out and show that competition between FM and AFM interactions leads to the appearance of quasielastic scattering for all momentum transfers. In addition, critical FM scattering grows as the temperature approaches T_c from above, which, surprisingly, is accompanied by the growth of low-energy AFM correlations. These results were understood in terms of FM polarons in the presence of strong AFM fluctuations arising from the superexchange interaction between t_{2g} spins, and were found to be at least in semiquantitative agreement with experimental results available at that time.[25]

Here, we report on measurements for the dynamics of doubly doped perovskites of general formula $La_{0.7}Pb_{0.3}(Mn_{1-x}Fe_x)O_3$, $0 \leqslant x \leqslant 0.2$ (LPMFO), carried out within the nanosecond time scales by means of neutron spin-echo (NSE) spectroscopy. Our main aim is to shed some light on the effects of magnetic frustration on the stochastic spin dynamics in a controlled way by means of increasing the number of broken bonds within the double exchange (DE) chains, which is achieved by means of Fe doping. The measurements have been carried out aiming to unravel the mechanisms giving rise to the complex relaxation patterns revealed by muon spectroscopy.[26] To such an avail, use will be made here of the rather different frequency windows accessible to NSE and we will derive some geometric information concerning the spatial dependences of the observed relaxations by means of wave-vector-dependent studies of the relaxation parameters.

The LPMFO system is highly frustrated. The hole concentration is well beyond the universal percolation threshold $x_c \approx 0.17$,[6] which leads to an insulator→semiconductor transition at some $T_{I\rightarrow SC}$, which significantly departs from T_c as the Fe concentration increases[27] and leads for $x \geqslant 0.15$ to purely insulating states. Iron enters the perovskite structure as Fe^{+3} as proven by Mössbauer spectroscopy,[28] whereas the FM character mainly arises from double exchange interactions between Mn^{3+} and Mn^{4+} ions. Doping with Fe into Mn sites, thus, leads to strong frustration since DE bonds are progressively broken as Fe concentration increases, leading for $x=0.2$ to a spin-glass-like state devoid of magnetic long-range order. This results from the action of a fully filled e_g band of Fe, which leads to a reduction of hopping sites since Fe^{3+} depletes the ratio of Mn^{3+}/Mn^{4+}. Doping with a transition metal such as Fe allows one to follow the effect of magnetic frustration in a controlled manner since the lattice distortion due to a change in ion size is minimal. The issue is of interest for two reasons. First, addition of 10% Fe ($x=0.1$) leads to a strong enhancement of the CMR effect.[27] Second, and on a more fundamental vein, lowering of the Curie temperature which is achieved by increasing Fe doping can also result from the introduction of significant cation disorder[29] via changes in size of cations surrounding the manganese ions, but leaving the nature of the magnetic interactions unchanged. Our results, thus, may serve to quantify the effects of disorder versus magnetic frustration on the reduction of T_c.

Structural studies on these samples[30] portray their magnetic structure within their paramagnetic (PM) region as constituted by relatively large $d \approx 8$ nm ferromagnetic regions, which order macroscopically below T_c, as well as smaller sized $d \approx 3$ nm AFM regions. As T_c is approached from above, critical FM scattering develops and shows a divergencelike behavior of its correlation length $\xi(T)$ concomitant with a small jump in density of the FM ordered regions. Both $\xi(T)$ and the parameter values characterizing the FM clusters, such as their diameter and density n, depend on the Fe content. The parent compound displays a sharp transition at T_c, whereas increasing the Fe content significantly smears out such a transition. The picture just sketched is usually understood as arising from the strong exchange coupling between spins in these materials. The expectancy is to find the carriers localized within such FM clusters. It is precisely because of this short-range order that a magnetic potential well is created, and this may be able to trap the carriers due to Hund's coupling, which aligns the core spins with the conduction electron spins. The entities just described are usually referred to as free magnetic polarons,[31] which are deemed to exist provided the density of carriers n_c fulfills $n_c \ll \xi^{-3}$.

Our first studies on the dynamics of LPFMO manganites[26,32] followed some preliminary ac susceptibility measurements[33] which revealed rather complicated spectral patterns as the Fe concentration increased. The muon spin relaxation rates as well as the associated signal intensity displayed a systematic trend[26] which goes from that characteristic of a simple ferromagnet, exhibited by the $La_{0.7}Pb_{0.3}MnO_3$ parent compound upon crossing the ordering temperature, to that shown for the $x=0.2$ sample, which displayed a sluggish transition at T_c followed by additional relaxation phenomena at significantly lower temperatures. The results did show a systematic trend with Fe content. Concentrations of $x=0.1$ did have a dramatic effect on the relaxation

patterns, which correlates with changes observed in macroscopic magnetization measurements. The highly doped $x=0.2$ sample did merit to delve some additional attention since, here, the relaxation was clearly nonexponential and the best fits involved two exponentials with well separated decay constants. The relaxation rates associated with both components did show rather disparate temperature dependences, the faster displaying a divergencelike behavior accountable in terms of a Tamann-Vogel-Fulcher function, while the slower rate displayed a far milder behavior with temperature. To set some characteristic time scales, recourse to fast-fluctuation limiting behavior concerning the Mn spin fluctuation rates is made. This means that $\Gamma_{\mathrm{Mn}} \gg \omega_\mu$, where Γ_{Mn} stands for the Mn spin fluctuation rates and ω_μ is set as a reference to the value of the low-temperature muon spin resonance frequency as found for LCMO,[23] $\omega_\mu = 4.7 \times 10^8$ rad/s. Using such a reference frequency and those taken from the muon relaxation rates close to T_c,[26] we get estimates for the fluctuation rates for Mn spins Γ_{Mn} of 3.2×10^{12}, 6.3×10^{11}, 4.4×10^{11}, and 5.5×10^{10} s^{-1} for Fe concentrations $x=0$, 0.1, 0.15, and 0.2, respectively. Such figures, thus, suggest that further insights into the spin dynamics of these materials could be gained by means of high-resolution neutron spectroscopy. In fact, preliminary results[32] from fixed-window measurements yielded information on the temperature dependence of the total intensity entering a frequency window of about $\omega \pm 5$ μeV for $x=0.2$, displaying a rather sluggish transition reminiscent of glassy phenomena. Most of the intensity was, however, concentrated at the low-angle detector banks, and individual spectra could not be separated due to insufficient statistics. On the other hand, kinematic limitations hamper the resolution of the spectra into frequency components, and therefore, measurements using lower momentum transfers were needed.

II. EXPERIMENTS

The samples were synthesized by the sol-gel method,[27] which yields finely divided powders with compositions $La_{0.7}Pb_{0.3}(Mn_{1-x}Fe_x)O_3$, $0 \leqslant x \leqslant 0.2$. The averaged grain sizes as determined by transmission electron microscopy came to be of about 100 nm for the Fe undoped composition, and ranging from 80 to 50 nm as the Fe content is increased. Such grain sizes ensure that phenomena here reported correspond to those exhibited by the bulk material since a previous determination of magnetic inhomogeneities by means of small-angle neutron scattering (SANS) and polarized neutron diffraction[30] has set a bound of 8 nm as the maximum diameter for the magnetic short-range-ordered entities which persist well within the PM phase.

Structurally, compositions below $x=0.2$ attain magnetic long-range order below a macroscopic ordering temperature, which decreases with increasing Fe content, that is, $T_c = 350$, 230, and 160 K for $x=0$, 0.1, and 0.15, respectively. This is accompanied by a decrease of spontaneous magnetization, which shows values for the magnetic moment as determined from macroscopic magnetometry measurements of $3.6\mu_B$, $2.9\mu_B$, and $2.4\mu_B$ for the same compositions. Such values are in very good agreement with the expectancy of antiferromagnetic coupling of Fe^{+3} to Mn, which holds for all these compositions. Our view of the magnetic structure of these samples is grounded on previous analysis of SANS data in terms of a liquid droplet model,[5,30] where FM short-range-ordered regions of some 8 nm in diameter, which are separated by distances of about 12 nm, collectively reorient below T_c, yielding ordered domains having a size of about 20 nm which, in turn, will interact between themselves, leading to the appearance of spontaneous magnetization. Fe concentrations of $x=0.2$ and beyond hamper the attainment of a long-range-ordered state via inhibiting the formation of the larger domains. Magnetic ordering yielding a moment of $1\mu_B$ can, however, be achieved by the action of external fields as low as 0.5 T. In all cases, a fully ordered state is never achieved, as witnessed by the presence of magnetic diffuse intensity down to temperatures well within the FM region. The effect of the addition of Fe is mostly felt by the packing densities, which decrease from $\eta=0.49$ for the parent compound to a loosely packed structure with $\eta=0.32$, an effect which is accompanied by a strong enhancement of the CMR effect.[27] In contrast, the crystal lattices expand uniformly up to about 0.5% with the introduction of up to $x=0.2$ of Fe, leaving the relevant angles unchanged. In real numbers, the $Q3$ orthorhombic distortion varies from 0.288 for the parent compound to a mere 0.292 for $x=0.2$

Compositions with $x \geqslant 0.15$ behave as electrical insulators down to the lowest explored temperatures (20 K). In contrast, samples with $x=0$ and 0.1 show a semiconductor $\rightarrow$insulator transition at temperatures significantly below that signaling the onset of magnetic ordering.[26]

Preliminary NSE data were taken at Forschungzentrum Jülich, Germany, using an incident wavelength $\lambda = 8$ Å. These measurements served to set the optimal instrument conditions to be used in the detailed study carried out using the neutron spin-echo machine IN11 at the Institut Laue-Langevin, Grenoble, France. The instrument was set up using an incident wavelength $\lambda = 7.2$ Å and scattering angles between 1.97° and 8°. This allowed us to explore a region of momentum transfers within $0.03 \leqslant Q \leqslant 0.12$ $\mathrm{Å}^{-1}$, which corresponds to the region comprising the low-angle region previously reported from neutron small-angle scattering as well as most of the small-angle-scattering intensity of magnetic origin previously studied by fully polarized neutron diffraction.[30]

Particular care was taken on data correction steps to allow for the substantial beam depolarization effects resulting from the development of a strong FM component, which become very strong at temperatures well below T_c, an effect that became particularly severe for the undoped or lightly doped samples.

Because of the limitations in the available frequency windows as well as the beam depolarization at temperatures well below T_c, our measurements are necessarily limited to temperatures about that comprising the transition to the macroscopically ordered state.

III. RESULTS

Figure 1 depicts results for the undoped and $x=0.2$ samples. Visual inspection of both sets of curves reveals a

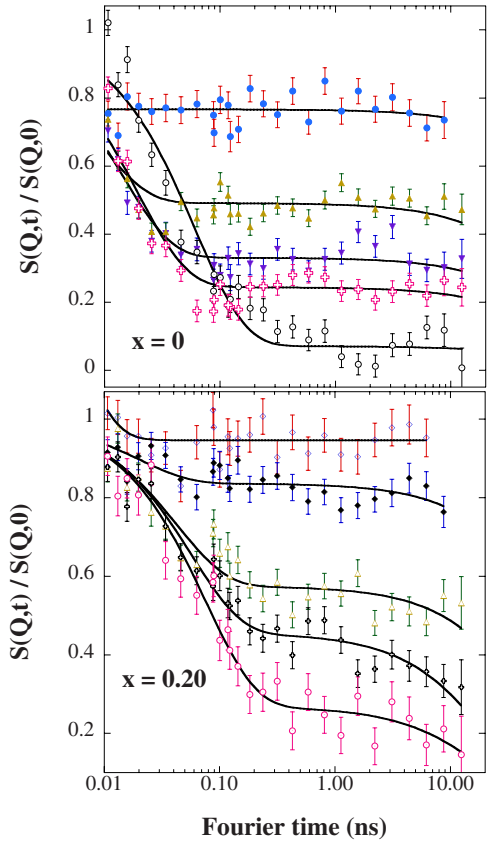

FIG. 1. (Color online) The upper frame depicts NSE spectra for the $La_{0.7}Pb_{0.3}MnO_3$ parent compound for several temperatures and $Q=0.03$ Å^{-1}. Temperatures are $T=300$, 340, 345, 347.5, and 350 K, from top to bottom. The lower frame displays data for $x=0.2$ and temperatures of 30, 45, 60, 70, and 100 K, from top to bottom. In both cases, lines depict fits to Eq. (1).

strong departure from a single-relaxation process, which becomes largely enhanced for the Fe-doped sample. Because of the rather low wave vectors here being explored, 0.03 Å^{-1} $\leqslant Q \leqslant$ 0.12 Å^{-1} hydrodynamic exponential response functions rather than Gaussians are deemed adequate to describe the spectral shape. Moreover, departure from exponential relaxation is usually accounted for in terms of either the presence of more than one relevant time scale or because of the emergence of genuinely complex phenomena such as those exhibited by spin glasses, where it is assumed that the relaxation times rather than single quantities are distributed following some prescribed distribution functions[34] which yield the widespread stretched-exponential law $\phi(t) \propto \exp[(-t\lambda_{KWW})^{\beta}]$. Alternative derivations for the stretched exponential or Kolhrausch-William-Watts (KWW) function, all of them derived on phenomenological grounds, include the assumption of relaxation processes ending up in randomly distributed static traps,[35] a distribution of relaxation rates that depend on sizes of the relaxing units,[36] the presence of competing exponential behavior in finite systems,[37] or the dynamics of fully frustrated Ising models.[38]

Our aim, thus, consists in modeling the spectra for all compositions in terms of relaxation patterns as simple as possible, with parameters having a definite physical meaning. As mentioned above, single-exponential or Gaussian relaxation functions are ruled out from the outset in view of the clear departure from linearity if $S(Q,t)/S(Q,0)$ is plotted on a logarithmic scale. A stretched-exponential function of the form $S(Q,t)/S(Q,0)=\exp[(-t\lambda_{KWW})^{\beta}]+B$ can only fit the data if a constant background term B is added to account for the unrelaxed part of the spectrum. Alternatively, the simplest approximation able to account for the data using a minimum of adjustable parameters considers two individual relaxation processes with decay rates λ_1 and λ_2, and a single amplitude parameter A, that is,

$$S(Q,t)/S(Q,0) = A\,\exp(-\lambda_1 t) + (1-A)\exp(-\lambda_2 t), \quad (1)$$

which involves the same number of adjustable parameters as the stretched exponential. Both relaxation rates can, thus, be assigned to specific decay channels for magnetic fluctuations since contributions from the structural degrees of freedom (phonons or diffusionlike processes) are deemed to lay well outside of our frequency window.

Figure 2 exemplifies the relative merits of both fitting functions. As shown there, the best fit using a single relaxation (KWW approximation) leads in some cases to values for the stretching exponent $\beta \approx 1$, telling us that a single exponential plus a background term fare equally well. As can be seen from the data shown in Fig. 2, both approaches are justified on statistical grounds since they yield fits of comparable quality. However, the main difficulty in pursuing the analysis using the KWW approximation stems from the need of accounting for the unrelaxed part of the spectrum, a quantity which becomes temperature, composition, and wave-vector dependent and cannot be easily ascribed to any definite physical entity.

The failure of a single-relaxation approach such as the KWW is easily understood since the curves shown in Fig. 1 do actually display two disparate dynamic regimes, which dominate the relaxation pattern below some 0.1 ns and above this, respectively. As we shall see below, exception made of the data for the $x=0$ composition close to T_c, the data does not show any clear features indicating the presence of finite-frequency excitations, an issue for which the discussion is deferred to Sec. IV. At any rate and in order to describe the effects of Fe doping on quantitative grounds, we will first consider all data on equal footing, even if the spectra for two temperatures close to T_c in the parent compound are best represented by the addition of an oscillatory component.

As shown in Fig. 1, Eq. (1) did provide an adequate representation of spectra for most measured temperatures and compositions, which enables us to discuss the effects of Fe doping on quantitative grounds.

The temperature dependence of the characteristic relaxation rates and the normalized amplitude parameter obtained for all samples are displayed in Fig. 3, and a summary of the derived values for the relaxation rates and fractional amplitudes for the two extreme temperatures of each composition is given in Table I. The data show that well within the paramagnetic region, values for the main relaxation rate λ_1 become strikingly close to a value of about 10 ns^{-1}, which point toward a common origin for this relaxation process irrespective of Fe doping. In contrast, the data for the lowest

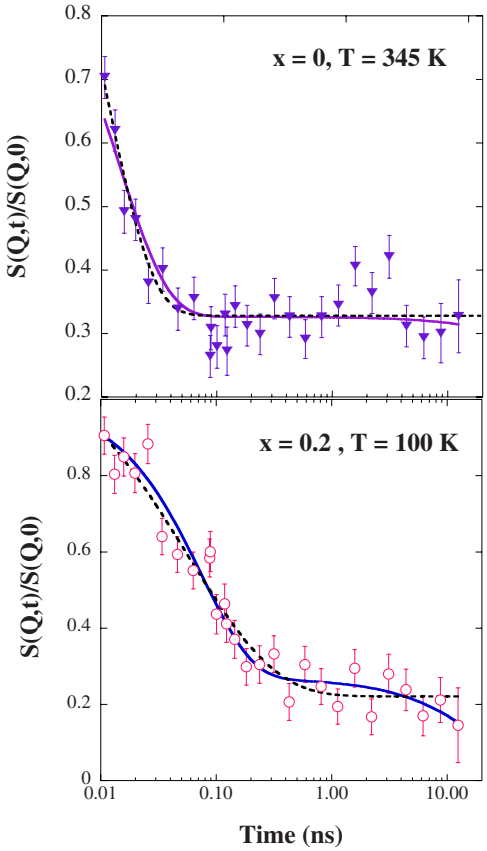

FIG. 2. (Color online) A comparison of the quality of single stretched-exponential relaxation (dashed) and two-relaxation-time (solid) approximations for data analysis of two selected spectra. The upper frame shows approximations for data pertaining to the parent compound, which yield parameters for the KWW of $\lambda_{KWW}=94(6)$ ns^{-1}, $\beta=1.1$ (2), and $B=0.327(7)$ and statistics $\chi^2=34.3$ and $R=0.929$, while the fit to Eq. (1) yields $\lambda_1=71(4)$ ns^{-1}, $\lambda_2=0.003(7)$ ns^{-1}, and $A=0.677(8)$ and statistics $\chi^2=40.6$ and $R=0.920$. The lower frame shows approximations for data on the $x=0.2$ doped compound, which yield parameters for the KWW of $\lambda_{KWW}=17(2)$ ns^{-1}, $\beta=0.57(4)$, and $B=0.22(1)$ and statistics $\chi^2=31.4$ and $R=0.973$, while the fit to Eq. (1) yields $\lambda_1=13.18(1)$ ns^{-1}, $\lambda_2=0.045(9)$ ns^{-1}, and $A=0.73(2)$ and statistics $\chi^2=32.0$ and $R=0.973$. Notice that B stands for a temperature- and wave-vector-dependent background term which needs to be included to fit the data using the KWW function.

explored temperatures, all of them below the macroscopic T_c, show a strong increase in value for the main rate. As far as the slower relaxation rate λ_2 is concerned, the figures listed in Table I tell of a separation in time scales of 2- and 4 orders of magnitude for the parent and doped compounds, respectively.

The graphs showing the temperature dependence of the relaxation rates displayed in Fig. 3 reveal the following features. First, both the relaxation rate and the amplitude for the faster exponential relaxation used to describe the data for the $La_{0.7}Pb_{0.3}MnO_3$ parent compound follow the trend that could be expected for a ferromagnet as T_c is approached from above. The relaxation rate displays a divergencelike cusp in much the same way as it was observed using muon

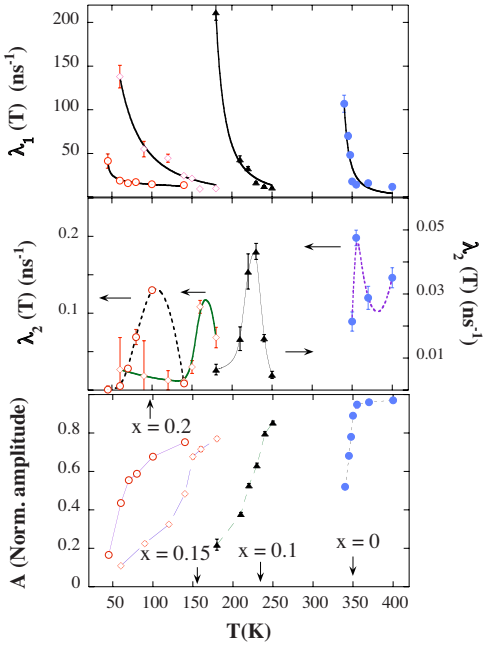

FIG. 3. (Color online) The figure shows the temperature dependence of the two relaxation rates. The upper frame depicts the results for the fast $\lambda_1(T)$ rate. Sample compositions range from $x=0$ (filled circles), $x=0.1$ (filled triangles), $x=0.15$ (open lozenges), and $x=0.2$ (open circles with a dot). The lines joining the data are best fits to functional forms $\lambda=D(T/T^*-1)^{-w}$ (see text). The middle frame shows data for λ_2. Lines are drawn as guides for the eye. Notice the rather different scales used to plot $x=0$ and $x=0.2$ versus $x=0.1$ and $x=0.15$. The lower frame shows the temperature dependence of the amplitude parameter A for the fastest relaxation. Lines drawn through the data are guides for the eye. The arrows mark the macroscopic ordering temperature for each individual composition.

spectroscopy,[26] which is accompanied by a loss in signal strength as temperature is lowered. To compare data on numerical grounds, here, we follow the same steps taken for the analysis of muon data in Ref. 26, where the relaxation rate was fitted by a power law[39]

$$\lambda_1 = D\left(\frac{T}{T^*}-1\right)^{-w}. \tag{2}$$

Here, D and w stand for critical parameters, which can be calculated in full for some model systems.[39] As shown in the uppermost frame of Fig. 3, the data for the parent compound can be accounted for if T^* is identified with the blocking temperature $T_p=330$ K given by zero-field cooled and field cooled curves,[26] and $w=1.5$ as predicted for isotropic Heisenberg magnets.[39] A single parameter fit to Eq. (2) yields $D=0.55\pm0.05$ ns^{-1}. The procedure also serves to account for the data for the Fe-doped samples, although identification of T^* with the blocking temperature cannot be made, and thus, T^* is left as an adjustable parameter. In doing so, one gets values for T^* of 160, 60, and 44 K for $x=0.1$, 0.15, and 0.2, respectively, which are 40, 60, and 16 K below the corresponding T_p as determined by magnetometry. Data concerning $x=0.2$ do, however, show a significant change in pattern

TABLE I. Estimated values for the relaxation rates and amplitudes as well as the activation parameters within the paramagnetic region. Numerical data for the measured relaxation rates are given for the two extreme temperatures measured for each composition. Estimated parameter errors are given in parentheses.

Composition (% Fe)	T/T_c	λ_1 (ns^{-1})	λ_2 (ns^{-1})	A	λ_0 (ns^{-1})	E_0 (meV)
0	1.143	11.7(4)	0.15(1)	0.970(9)	$2.15(4)\times10^{-3}$	288.7(3)
0	0.971	107(9)		0.520(6)		
0.10	1.087	11.15(29)	0.0064(17)	0.855(8)	$4.32(6)\times10^{-3}$	167.2(5)
0.10	0.783	211(91)	0.0048(11)	0.219(3)		
0.15	1.125	9.86(34)	0.0164(32)	0.77(1)	0.45(1)	48.0(6)
0.15	0.375	138(73)	0.006(9)	0.109(7)		
0.20	1.474	13.8(3)	0.008(2)	0.853(6)	10.94(4)	2.75(3)
0.20	0.474	41(8)	0.0006(9)	0.166(7)		

since a far smaller value for the critical exponent $w=0.3$ was needed to account for the temperature dependence of its relaxation rate.

Data shown in Table I concerning the slower relaxation show that for the parent compound, it samples fluctuations with time scales some 80 times slower than the main, faster component. Its temperature dependence could only be followed down to T_c, and therefore, it could not be assessed whether it did exhibit any significant pattern at lower temperatures. In stark contrast, the Fe-doped samples show relaxation rates with even more disparate time scales, now involving differences of up to 4 orders of magnitude.

The most significant feature concerning λ_2 for all the samples concerns their striking nonmonotonous dependence with temperature. In all three cases, the slower relaxation rate exhibits a clear maximum, which appears at roughly the same temperature as the macroscopic T_c. The shape of these curves compare favorably to that followed by the main peak in the temperature dependence of the zero-field muon relaxation rates reported in Ref. 26 as well as with the temperature dependence of the intensity of the low-angle static structure factor $S(Q)$ at wave vectors comprising those, $0.02\ \text{Å}^{-1} \leqslant Q \leqslant 0.04\ \text{Å}^{-1}$, where it shows a broad maximum arising from the interactions of FM domains.[5,30]

Data shown in the lower frame of Fig. 3 display the temperature dependence of the amplitude of the main relaxation. In all cases, the amplitude associated with the λ_1 relaxation increases with increasing temperature, whereas, by construction, the strength of the slower component having a rate λ_2 increases as T_c is crossed from above. The curve for $A(T)$ follows for $x=0$ a narrow sigmoid shaped curve having T_c located at midrange. The shape of $A(T)$ becomes increasingly distorted with increasing Fe doping although, in all cases, T_c sits close to the midrange of such curves. Also notice that the maximal value for A well within the PM state also depends on Fe content, which means that the volume fraction associated with λ_2 increases with Fe content. The curves, however, seem to have a high-temperature common asymptote, which could not be ascertained due to the limitations in the frequency window of our technique.

To compare in some more detail the effects of Fe doping on the dynamics, we have considered in some more detail data for λ_1 within the PM region. From there, some insights into the energetics of the dynamic processes being sampled are provided by graphs shown in Fig. 4, where the measured data for λ_1 within the paramagnetic region are analyzed in terms of an Arrhenius law, from where an estimate for an activation energy E_0 and a frequency term λ_0 can be derived.

A glance to the upper frame of Fig. 4 reveals the remarkably strong compositional dependence of the slope of $\ln \lambda_1(x,T)$ versus the inverse temperature. The parameter values for the frequency factor λ_0 and the activation energy term E_0 are shown in the lower frame of Fig. 4 and the

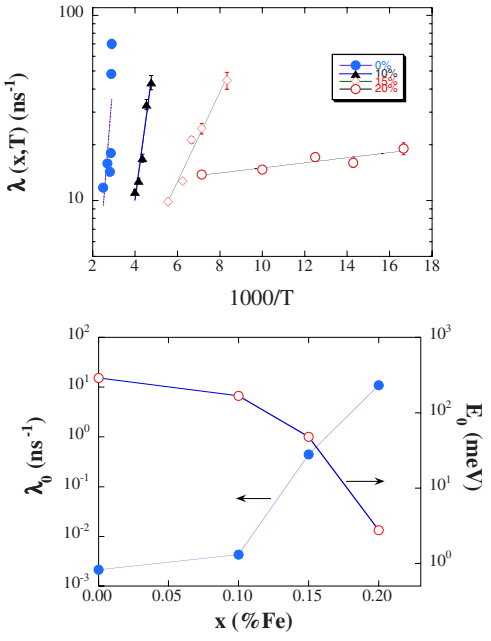

FIG. 4. (Color online) The upper frame depicts the relaxation rates plotted versus the inverse temperature for all the three compositions, which have been fitted to an exponential temperature dependence $\lambda(x,T)=\lambda_0 \exp(E_0/T)$. Symbols from left to right represent the parent compound and increasing Fe doping, and the straight lines are fits to the data. The composition dependence of the preexponential λ_0 and the activation energy terms E_0 are displayed in the lower frame (symbols). Lines drawn through the points are guides for the eye.

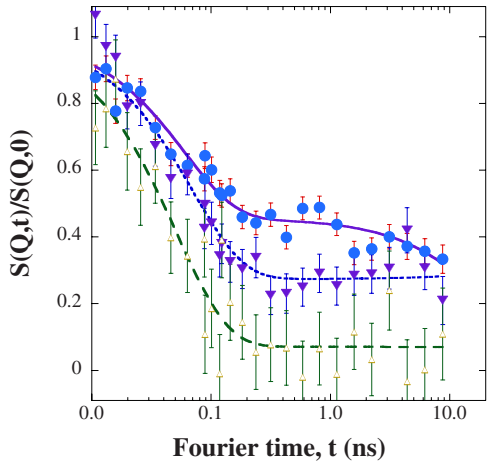

FIG. 5. (Color online) Wave-vector dependence of spectra for the $x=0.2$ sample at $T=70$ K. Data are shown for $Q=0.030$ Å^{-1} (filled circles), $Q=0.061$ Å^{-1} (filled inverted triangles), and $Q=0.091$ Å^{-1} (open triangles). Lines drawn through the points are approximations using two relaxation times given by Eq. (1).

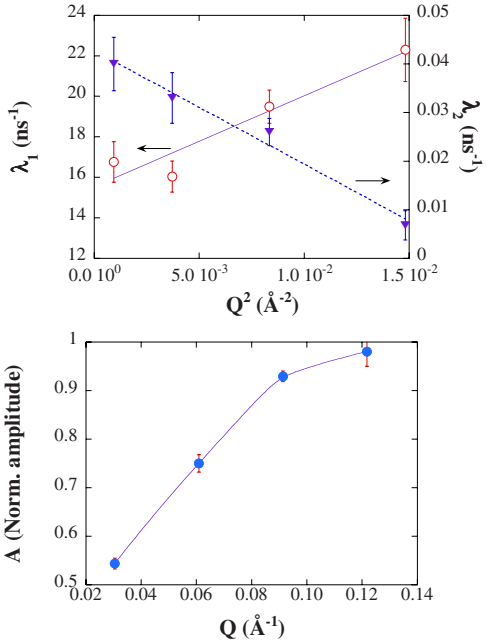

FIG. 6. (Color online) The upper frame displays the dependence of the relaxation rates with wave vector squared. Open circles with a dot show data for λ_1, and inverted triangles depict those for λ_2. Straight lines display fits yielding $\lambda_1=15.5+449Q^2$ and $\lambda_2=0.042-2.33Q^2$, respectively. The lower frame displays the wave-vector dependence of the amplitudes. Line drawn through the data is a guide for the eye. Both frames correspond to the $x=0.2$ sample at $T=70$ K.

pertinent data are listed in Table I. The most striking result coming out from such an exercise stems from the disparate values obtained for the frequency factor λ_0. In fact, there we see a transition from a full microscopic regime where λ_0 lies within the inverse picosecond range for the heavily doped compound to a state where λ_0 enters the inverse nanosecond range for the parent compound. Concomitantly, the energy term plummets from a value of $E_0 \approx 289$ meV, which is the same order of magnitude as those reported for spin-stiffness constants, down to $E_0 \approx 2.8$ meV for $x=0.2$.

One of the main advantages offered by neutron spectroscopies if compared to macroscopic or muon relaxation techniques consists in the possibility of accessing directly geometric information about atomic or spin motions by means of selecting different values of the observation wave vector. This route has also been followed here, and the Q dependence of some of the spectra is shown in Fig. 5. A glance to such curves shows that the spectra exhibit at low angles a significant wave-vector dependence. To quantify such behaviors, we have displayed the Q dependence for the parameters characterizing both relaxations in Fig. 6. Notice that measurements at momentum transfers beyond $Q=0.12$ Å^{-1} were not attempted due to the strong decrease in intensity (see Refs. 5 and 30). The Q dependence of λ_1 follows an apparent quadratic behavior with momentum transfer, with a finite intercept at $Q \to 0$, which is suggestive of some diffusionlike or spin-wave processes. In contrast, the relaxation rates for the slower component appear to decrease with increasing wave vector, which would imply that motions sampled by such relaxation are of collective nature since one would expect an increase of the relaxation rate with increasing Q otherwise. Furthermore, the fact that the amplitude $(1-A)$ for the slower relaxation follows the same trend as the static structure factor $S(Q)$ tells us that the relaxation rate and amplitude for λ_2 should be associated with processes having characteristic length scales compatible with those found for the FM entities.

As mentioned at the beginning of this section, some data pertaining to the parent compound close to T_c did show some indication of the presence of a heavily damped oscillatory component. A deeper insight into the nature of these relaxations is provided by a careful consideration of the line shapes of spectra for temperatures approaching T_c from below. In fact, data for $x=0$ and temperatures of (T_c-10) and $(T_c-2.5)$ are better reproduced, allowing for a finite-frequency excitation than in terms of a purely relaxational process. As a matter of fact, better fits to such spectra are given by

$$S(Q,t)/S(Q,0) = A\cos(\omega_c t + \phi)\exp(-\lambda_1 t) + (1-A)\exp(-\lambda_2 t), \quad (3)$$

where ω_c stands for the oscillation frequency, ϕ is a phase term, and λ_1 is identified here with the damping coefficient. An example of the quality of such fits is given in Fig. 7.

The characteristic frequencies from such an oscillation turned out to be 129 ns^{-1} for $(T_c-10$ K) and 29.4 ns^{-1} for $(T_c-2.5$ K), respectively. Data for temperatures about T_c or above did not show any evidence of oscillatory behavior. In addition, all the Fe-doped compositions did not show evidence of any finite-frequency excitation below the respective T_c. As we will discuss below, such values for the excitation frequencies are not far from others reported in the literature, and on such grounds, we assign the origin of the fast relaxation to heavily damped or overdamped spin waves.

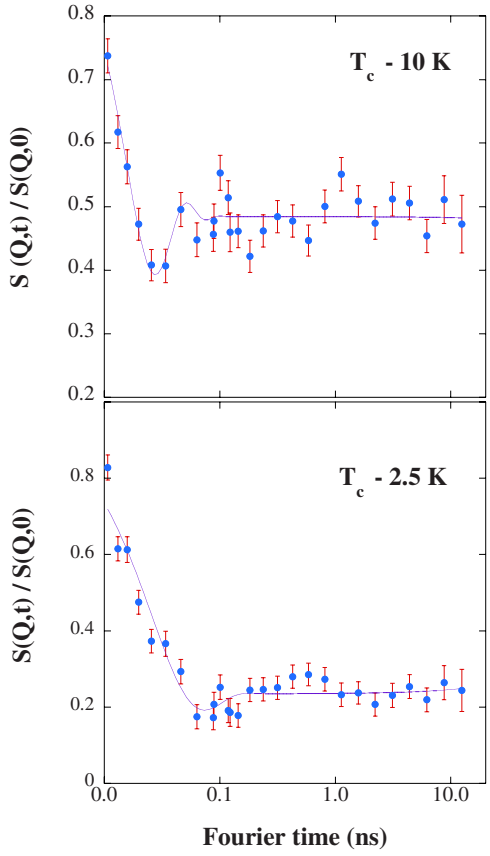

FIG. 7. (Color online) Spectra for the parent compound and the approximation given by Eq. (3) for the two temperatures given as insets relative to T_c=350 K.

IV. DISCUSSION AND CONCLUSIONS

Our main experimental finding concerns the presence of two well separated time scales which show significantly different wave-vector and temperature dependences. An indication of clear nonexponential relaxation was already noticed in our previous muon relaxation study,[26] although it was only apparent for the sample having 20% Fe (x=0.2). The current results, thus, extend the validity of such a finding to all the LPMFO series here studied.

The assignment of the fast-relaxing λ_1 to heavily damped or overdamped spin waves made above is further supported by comparison of the oscillation frequencies found just below T_c, as shown in Fig. 7, to reported data for the stiffness constants determined in detailed studies on single crystals of some other CMR compounds.[17,40,41] Such frequencies that are 129±20 ns^{-1} for (T_c−10) and 29±5 ns^{-1} for (T_c−2.5), with decay constants of 29±9 ns^{-1} and 33±12 ns^{-1}, respectively, can be cast in terms of polycrystalline averages of stiffness constants assuming that the hydrodynamic D_sQ^2 law holds and Q=0.03 Å^{-1}. The values derived for the two temperatures are D_s=94 meV Å^{-2} for (T_c−10) and 21.5 meV Å^{-2} for (T_c−2.5), and correspond to heavily damped motions which become overdamped as T_c is crossed from below. Above T_c and within all the explored range of temperatures for the Fe-doped compounds, the spectrum of fast magnetic fluctuations is dominated by purely diffusive spin motions characterized by spin-diffusion constants given by $D_d=\lambda_1/Q^2$. Put into different words, here, we see that replacement of the Mn sites with Fe introduces an additional source of scattering of spin waves, which involves a further reduction of their lifetimes, leading to purely overdamped (i.e., quasielastic) motions. Such an assertion is also supported by preliminary estimates of the spin-stiffness constants at T=10 K derived from macroscopic magnetization measurements.[42] These show a dramatic reduction up to some 60% on the value of $D_s(x,T=10\ \mathrm{K})$ upon addition of 10% Fe (x=0.1). Such a reduction explains the absence of any finite-frequency feature in the spectra of Fe-doped samples since the damping terms as given by λ_1 would become larger than the spin-wave frequencies. A similar reduction of the spin-wave stiffness constant has been reported for Ni doping.[43] Moreover, substitution of Mn by Fe^{3+} also results in promoting a magnetically frustrated ground state with strong AFM correlations.

The analysis of the temperature dependence of $\lambda_1(T)$ also shows that Fe doping involves a very large reduction in the activation energy barriers for spin diffusion as well as an increase of several orders of magnitude of the attempt frequency. The characteristic values for the activation energy for spin diffusion within the heavily doped Fe samples are within the order of magnitude of diffusionlike processes that take place in highly disordered matter. The results are reminiscent of some previous attempts to describe the quasielastic intensity of $La_{2-2x}Sr_{1+2x}Mn_2O_7$,[21] which develops above some freezing temperature concomitantly with the onset of very strong phonon damping in terms of some glasslike behavior.

The temperature dependence of the slower λ_2 relaxation rate displays some features similar to those shown by a longitudinal muon relaxation rate measured under zero field.[26] It shows a maximum located at a temperature which roughly coincides with T_c. Its characteristic frequencies comprise scales within 10–200 MHz, which are also accessible to pulsed muon techniques, and thus, both techniques are sampling the same phenomena.

The highly doped compound x=0.2 merits some special consideration. As previously reported,[26,30,33] AFM spin correlations end up preventing the achievement of a long-ranged spin-ordered state. A FM ordering can, however, be induced under low fields, and the macroscopic ac susceptibility shows a number of characteristics common to those known to be characteristic of spin glasses.[33] Our results for such a composition resemble those reported for a single crystal of $La_{0.66}Ba_{0.40}Mn_{0.61}Fe_{0.33}O_3$,[44] where the presence of orbital correlations of $Mn^{3+}e_g$ electrons surviving within a largely perturbed magnetic environment is invoked to explain the origin of such a highly peculiar magnetic state.

As far as how pertinent the present findings may be to understand the CMR effect, it is worth recalling that this is maximum for x=0.10 and negligible for x=0.20. As mentioned previously,[26,27] the maximum enhancement of the magnetoresistance with respect to the parent $La_{0.7}Pb_{0.3}MnO_3$ corresponds to our lightest doped compound, and it is accompanied by a significant decrease in packing of FM entities as well as by an increase in their average size. Our re-

sults for the fastest relaxing component λ_1, well within the PM region where a common time scale is found for all the compounds, tell us that such overdamped motions *per se* bear little relevance to understand the CMR effect. The energetics of such motions, which monitors a drop in activation energy for the $x=0.1$ sample close to 40%, may, however, give some clues about an optimal range of particle inhomogeneities to generate the CMR phenomenon. In fact, from Table I, we see that further increases in Fe content beyond $x=0.1$ lead to larger AFM regions, which actually revert that trend. In contrast, the motions sampled at longer time scales by λ_2 as well as by the muon relaxation results seem to be more intimately connected with the underlying physics governing the CMR effect. From the data on the Q and temperature dependences of the λ_2 relaxation, we see that motions sampled at such time scales by muon and NSE spectroscopies deal with the average spins of nanoscopic objects, which align themselves to achieve a FM state. Also, notice that both diffraction and dynamics experiments monitor how the FM fraction increases upon crossing T_c from above.

The data here reported show some analogies with previous studies on relatively fast fluctuations[14,21,25,45] as manifested by a broad quasielastic scattering signal that coexists with spin-wave dispersions below T_c. Most of the discussion on such results, measured on $La_{0.75}(Ca_{0.45}Sr_{0.55})_{0.25}MnO_3$,[45] ascribe to dynamic, single uncorrelated polarons the dominant character of the quasielastic signal, as well as to polaron correlations the presence of a narrower quasielastic component. The lifetimes of both kinds of dynamic correlations were derived from the inverse of the quasielastic linewidths, which yield 120 and 600 fs, respectively. Our results, once cast into the same form, yield lifetimes of $\tau_1=63$ fs corresponding to λ_1, and thus, are in qualitative agreement with those reported in Ref. 45. The assignment of such motions to specific phenomena generated by strong lattice distortions relies on the fact that strong Jahn-Teller effects leading to polaron formation are deemed to be important for temperatures near and above T_c, and in fact,[46] effects of orbital fluctuations need to be included for a proper description of the magnon dispersion relations. There are, however, a number of problems which, in our opinion, hamper reaching a definite assignment of the observations here reported to motions of free or bound polarons. In particular, the problem of a quantitative evaluation of such effects still remains, since estimates of the Jahn-Teller electron-phonon coupling constants in these materials can only be derived on the basis of qualitative arguments.[47,48] Such difficulties add up to conflicting reports concerning structural data,[8,49] which have recently put into question the role of the JT distortion in our understanding of the transport properties of these materials. As a result, we leave our discussion open to a description of the moving entities in terms of polarons or any other entities.

As regards related work on manganites of similar composition, preliminary studies have been carried on Nd-based perovskites of general formula $Nd_{0.7}Pb_{0.3}(Mn_{1-x}Fe_x)O_3, 0 \leqslant x \leqslant 0.2$. The interest in this material stems from previous reports[50] on $Nd_{1-x}Sr_xMnO_3$, which have evidenced the presence of different kinds of magnetic inhomogeneities that give rise to complex relaxation patterns akin to those of a magnetic glass. Our results for the above referred compound have revealed strikingly different properties[51] from those here described for the La-based material. Our samples do show additional ordering processes at temperatures below 10 K, mostly due to the action of the Nd moments.

In summary, the present study reports on two dynamic scales having far more disparate characteristic times than those previously reported for $La_{0.7}Ca_{0.3}MnO_3$.[23] The detailed study of the temperature and wave-vector dependence of both relaxation rates has evidenced that both processes, albeit of diffusive nature above T_c, sample rather different physics. From data and arguments given above, we tentatively assign the observed relaxations as arising from heavily damped propagating or overdamped spin motions as well as collective reorientations of the total spins of FM ordered inhomogeneities which survive within the PM phase.

ACKNOWLEDGMENTS

J.G. and J.M.B. thank the Spanish Ministerio de Educacion y Ciencia for financial support under research Grant No. MAT2005-0686-C04-03. F.J.B. and P.R. acknowledge financial support from the European Commission through NMI3 to carry out preliminary measurements at the FZJ facilities.

*javier@langran.iem.csic.es

[1] G. Van Tendeloo, O. I. Levedev, M. Hervieu, and B. Raveau, Rep. Prog. Phys. **67**, 1315 (2004).

[2] E. Dagotto, T. Hotta, and A. Moreo, Phys. Rep. **233**, 1 (2001).

[3] See, for instance, Y. Okimoto, Y. Tomioka, Y. Onose, Y. Otsuka, and Y. Tokura, Phys. Rev. B **59**, 7401 (1999).

[4] J. C. Loudon and P. A. Midgley, Phys. Rev. Lett. **96**, 027214 (2006); S. Komiya, H.-D. Chen, S.-C. Zhang, and Y. Ando, *ibid.* **94**, 207004 (2005); T. Becker, C. Streng, Y. Luo, V. Moshnyaga, B. Damaschke, N. Shannon, and K. Samwer, *ibid.* **89**, 237203 (2002); C. D. Batista, J. M. Eroles, M. Avignon, and B. Alascio, Phys. Rev. B **58**, R14689 (1998); S. K. Mishra, R. Pandit, and S. Satpathy, *ibid.* **56**, 2316 (1997).

[5] N. Veglio, F. J. Bermejo, J. Gutiérrez, J. M. Barandiarán, A. Peña, M. A. Gonzalez, P. P. Romano, and C. Mondelli, Phys. Rev. B **71**, 212402 (2005).

[6] L. P. Gorkov and V. Z. Kresin, Phys. Rep. **400**, 149 (2004).

[7] See, for instance, M. Hennion and F. Moussa, New J. Phys. **7**, 84 (2005).

[8] E. S. Bozin, M. Schmidt, A. J. DeConinck, G. Paglia, J. F. Mitchell, T. Chatterji, P. G. Radaelli, T. Proffen, and S. J. L. Billinge, Phys. Rev. Lett. **98**, 137203 (2007).

[9] L. M. Woods, Phys. Rev. B **65**, 014409 (2001).

[10] T. G. Perring, G. Aeppli, S. M. Hayden, S. A. Carter, J. P. Remeika, and S.-W. Cheong, Phys. Rev. Lett. **77**, 711 (1996).

[11] C. P. Adams, J. W. Lynn, Y. M. Mukovskii, A. A. Arsenov, and

D. A. Shulyatev, Phys. Rev. Lett. **85**, 3954 (2000); V. Kiryukhin, T. Y. Koo, P. A. Sharma, J. P. Hill, and S. W. Cheong, Phys. Rev. B **64**, 220405(R) (2001).

[12] G. Biotteau, M. Hennion, F. Moussa, J. Rodriguez-Carvajal, L. Pinsard, A. Revcolevschi, Y. M. Mukovskii, and D. Shulyatev, Phys. Rev. B **64**, 104421 (2001).

[13] J. A. Fernandez-Baca, P.-C. Dai, H. Kawano-Furukawa, H. Yoshizawa, E. W. Plummer, S. Katano, Y. Tomioka, and Y. Tokura, Phys. Rev. B **66**, 054434 (2002).

[14] T. J. Sato, J. W. Lynn, and B. Dabrowski, Phys. Rev. Lett. **93**, 267204 (2004).

[15] M. Hennion, F. Moussa, G. Biotteau, J. Rodriguez-Carvajal, L. Pinsard, and A. Revcolevschi, Phys. Rev. B **61**, 9513 (2000); F. Moussa, M. Hennion, F. Wang, P. Kober, J. Rodríguez-Carvajal, P. Reutler, L. Pinsard, and A. Revcolevschi, *ibid.* **67**, 214430 (2003).

[16] Ch. Simon, S. Mercone, N. Guiblin, C. Martin, A. Brulet and G. Andre, Phys. Rev. Lett. **89**, 207202 (2002); S. Mercone, V. Hardy, C. Martin, Ch. Simon, D. Saurel, and A. Brulet, Phys. Rev. B **68**, 094422 (2003); L. P. Gorkov and V. Z. Kresin, Phys. Rep. **400**, 149 (2004).

[17] B. J. Kirby, J. J. Rhyne, H. Kaiser, H. Kuwahara, and Y. Tokura, J. Magn. Magn. Mater. **302**, 237 (2006).

[18] R. S. Fishman, Phys. Rev. B **70**, 012403 (2004).

[19] T. Chatterji, M. M. Koza, F. Demmel, W. Schmidt, J.-U. Hoffmann, U. Aman, R. Schneider, G. Dhalenne, R. Suryanarayanan, and A. Revcolevschi, Phys. Rev. B **73**, 104449 (2006).

[20] F. Ye, P. Dai, J. A. Fernandez-Baca, H. Sha, J. W. Lynn, H. Kawano-Furukawa, Y. Tomioka, Y. Tokura, and J. Zhang, Phys. Rev. Lett. **96**, 047204 (2006).

[21] D. N. Argyriou, J. W. Lynn, R. Osborn, B. Campbell, J. F. Mitchell, U. Ruett, H. N. Bordallo, A. Wildes, and C. D. Ling, Phys. Rev. Lett. **89**, 036401 (2002).

[22] R. Kajimoto, H. Yoshizawa, H. Kawano, H. Kuwahara, and Y. Tokura, J. Phys. Chem. Solids **60**, 1177 (1999).

[23] R. H. Heffner, J. E. Sonier, D. E. MacLaughlin, G. J. Nieuwenhuys, G. Ehlers, F. Mezei, S.-W. Cheong, J. S. Gardner, and H. Röder, Phys. Rev. Lett. **85**, 3285 (2000); R. H. Heffner, J. E. Sonier, D. E. MacLaughlin, G. J. Nieuwenhuys, G. M. Luke, Y. J. Uemura, W. Ratcliff II, S. W. Cheong, and G. Balakrishnan, Phys. Rev. B **63**, 094408 (2001).

[24] P. Horsch, J. Jaklic, and F. Mack, Phys. Rev. B **59**, R14149 (1999).

[25] T. G. Perring, G. Aeppli, Y. Moritomo, and Y Tokura, Phys. Rev. Lett. **78**, 3197 (1997).

[26] J. Gutiérrez, F. J. Bermejo, J. M. Barandiarán, S. P. Cottrell, P. P. Romano, C. Mondelli, J. R. Stewart, L. Fernández Barquin, and A. Peña, Phys. Rev. B **73**, 054433 (2006).

[27] J. Gutiérrez, A. Peña, J. M. Barandiarán, J. L. Pizarro, T. Hernandez, L. Lezama, M. Insausti, and T. Rojo, Phys. Rev. B **61**, 9028 (2000).

[28] J. M. Barandiarán, J. M. Greneche, T. Hernandez, F. Plazaola, and T. Rojo, J. Phys.: Condens. Matter **14**, 12563 (2002).

[29] J. Salafranca and L. Brey, Phys. Rev. B **73**, 214404 (2006).

[30] J. Gutiérrez, F. J. Bermejo, N. Veglio, J. M. Barandiarán, P. Romano, C. Mondelli, M. A. González, and A. P. Murani, J. Phys.: Condens. Matter **18**, 9951 (2006).

[31] P. Majumdar and P. B. Littlewood, Phys. Rev. Lett. **81**, 1314 (1998); T. Holstein, Ann. Phys. (N.Y.) **281**, 725 (2000).

[32] J. Gutiérrez, J. M. Barandiarán, F. J. Bermejo, A. Peña, J. J. Blanco, T. Rojo, L. Fernandez-Barquin, C. Mondelli, and M. A. Gonzalez, J. Magn. Magn. Mater. **272-276**, 983(E) (2004).

[33] For an account of the ac susceptibility for the $x=0.2$ composition, see L. Fernandez-Barquin and R. Garcia-Calderón, J. Phys.: Conf. Ser. **17**, 87 (2005).

[34] R. G. Palmer, D. L. Stein, E. Abrahams, and P. W. Anderson, Phys. Rev. Lett. **53**, 958 (1984).

[35] J. C. Phillips, Rep. Prog. Phys. **59**, 1133 (1996).

[36] R. V. Chamberlin, Phys. Rev. Lett. **82**, 2520 (1999).

[37] A. Bunde, S. Havlin, J. Klafter, G. Gräff, and A. Shehter, Phys. Rev. Lett.. **78**, 3338 (1997).

[38] A. Fierro, A. de Candia, and A. Coniglio, Phys. Rev. E **56**, 4990 (1997).

[39] L. Onsager, Phys. Rev. **65**, 117 (1944); G. F. Mazenko and O. T. Valls, *ibid.* **24**, 1419 (1981); C. Hohenemser, N. Rosov, and A. Kleinhammes, Hyperfine Interact. **49**, 267 (1989).

[40] J. A. Fernandez-Baca, P. Dai, H. Y. Hwang, C. Kloc, and S.-W. Cheong, Phys. Rev. Lett. **80**, 4012 (1998).

[41] F. Ye, Pengcheng Dai, J. A. Fernandez-Baca, D. T. Adroja, T. G. Perring, Y. Tomioka, and Y. Tokura, Phys. Rev. B **75**, 144408 (2007).

[42] Derived values from magnetometry measurements under low fields [J. Gutierrez (unpublished)].

[43] S. Pal, E. Bose, B. K. Chauduri, H. D. Yang, S. Neeleshwar, and Y. Y. Chen, J. Magn. Magn. Mater. **293**, 872 (2005).

[44] E. Granado, R. R. Urbano, C. A. Perez, C. Azimonte, J. W. Lynn, R. A. Souza, N. M. Souza-Neto, A. Y. Ramos, G. L. Bychkov, S. V. Shiryaev, and S. N. Barilo, Phys. Rev. B **72**, 052406 (2005).

[45] V. Kiryukhin, A. Borissov, J. S. Ahn, Q. Huang, J. W. Lynn, and S.-W. Cheong, Phys. Rev. B **70**, 214424 (2004).

[46] G. Khaliullin and R. Kilian, Phys. Rev. B **61**, 3494 (2000).

[47] E. L. Nagaev, Phys. Rep. **346**, 387 (2001).

[48] H. Meskine, T. Saha-Dasgupta, and S. Satpathy, Phys. Rev. Lett. **92**, 056401 (2004).

[49] H. Kugawara, Y. Tomioka, and A. Asamitsu, Science **270**, 961 (1996); D. Louca and T. Egami, Phys. Rev. B **59**, 6193 (1999).

[50] V. V. Krishnamurthy, I. Watanabe, K. Nagamine, H. Kuwahara, and Y. Tokura, Phys. Rev. B **61**, 4060 (2000).

[51] J. J. Blanco, Ph.D. thesis, University of the Basque Country, 2002.